energies

MDPI

Article

Self-Affine Analysis of ENSO in Solar Radiation

Thiago B. Murari [1,*], Aloisio S. Nascimento Filho [1], Marcelo A. Moret [1,2], Sergio Pitombo [1] and Alex A. B. Santos [1]

[1] Gestão e Tecnologia Industrial (PPG GETEC), Centro Universitário SENAI CIMATEC, Salvador 41650-010, BA, Brazil; aloisio.nascimento@gmail.com (A.S.N.F.); mamoret@gmail.com (M.A.M.); sergio.pitombo@fieb.org.br (S.P.); alex.santos@fieb.org.br (A.A.B.S.)

[2] Senai CIMATEC, Universidade do Estado da Bahia—UNEB, Salvador 41150-000, BA, Brazil

* Correspondence: mura.learning@gmail.com

Received: 10 August 2020; Accepted: 11 September 2020; Published: 15 September 2020

Abstract: The major challenge we face today in the energy sector is to meet the growing demand for electricity with less impact on the environment. South America is an important player in the renewable energy resource. Brazil accelerated the growth of photovoltaic installed capacity in 2018. From April of 2017 to April of 2018, the capacity increased by 1351.5%. It is expected to reach the value of 2.4 GW until the end of the year. The new Chilean regulation requests that 20% of the total electricity production in 2025 must come from renewable energy sources. The aim of this paper is to establish time series behavior changes between El Niño Southern Oscillation and the solar radiation resource in South America. The results can be used to validate the measured data of energy production for new solar plants. The method used to verify the behavior of the time series was the Detrended Fluctuation Analysis. Solar radiation data were collected in twenty-five cities distributed inside the Brazilian solar belt, plus six cities in Chile, covering the continent from east to west, in a region with high potential of solar photovoltaic generation. The results show the impact of El Niño Southern Oscillation on the climatic behavior of the evaluated data. It is a factor that may lead to the wrong forecast of the long-term potential solar power generation for the region.

Keywords: solar radiation; DFA; photovoltaic energy plant; ENSO

1. Introduction

Renewable energy sources may play an important role in solving the dilemma of increasing energy production capacity by minimizing the environmental impact [1]. Some studies have been investigated the potential contribution of renewable energy supplies to the global grid. It has been indicated that, in the second half of this century, their contribution might range from 20% to more than 50% once we establish the correct government policies [2]. That has encouraged a large number of studies, mainly in the photovoltaic energy field [3–6].

Regarding renewable energy investments, Brazil and Chile stand out in South America. Both are the first and second destination countries for foreign investment. According to the Ministry of Mines and Energy of Brazil (MME), the installed capacity of power generation in Brazil reached 150.4 GW in 2016, an increase of 9.5 GW in relation to 2015. Among the sources that stand out most are hydropower, with 64.5%, and biomass, with 9.3%. Considering this import source, the total power supply reached 156.3 GW in 2016.

In addition, according to the monthly monitoring bulletin of the Brazilian Electric System from MME, the solar photovoltaic source in Brazil has grown rapidly in recent years. Brazil reached the end of 2018 with 2400 MW. Further, the 10-year Energy Expansion Plan (PDE 2024) estimates that the installed capacity of solar generation in Brazil will reach 8300 MW by 2024.

A Certified Energy Production Estimate (CEPE) was requested for new projects in Brazil [7]. It was calculated based on twelve consecutive months of measurements within a radius of up to 10 km from the project. This local measured data were compared with the same period data obtained from satellite models to obtain the Typical Meteorological Year (TMY), which was used in the calculation of CEPE. Moreover, these certified data were correlated with a dataset collected from the closest weather station for 10 years or more.

Brazil has great potential for photovoltaic power generation. The Northeastern region has the highest potential of the country, with a mean solar Global Horizontal Irradiance (GHI) value of 5.9 kWh/m^2. Figure 1 shows a map of photovoltaic power generation. It presents the maximum annual energy yield (measured in kWh of annual energy generated by kWp of installed photovoltaic energy) for the entire Brazilian territory.

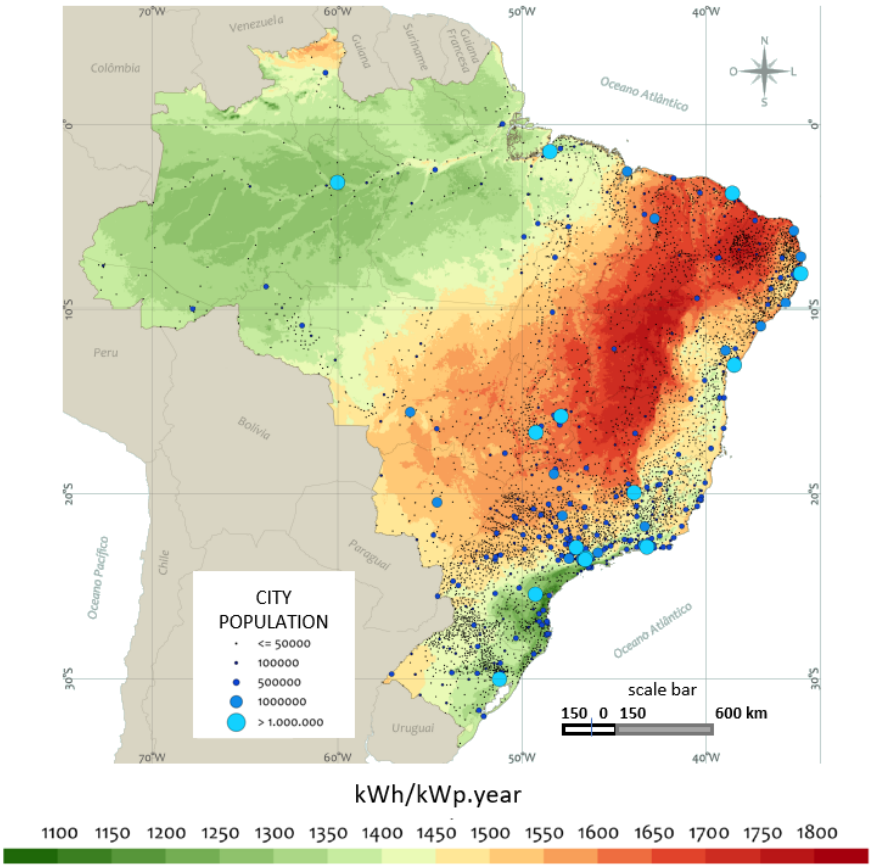

Figure 1. Photovoltaic power generation potential in Brazil. The size of the blue circles represents the number of inhabitants in each Brazilian city. Adapted from [8].

South America is impacted by the El Niño Southern Oscillation (ENSO). Both El Niño and La Niña climate phenomena are known as ENSO. They are the opposite phases of a natural climate pattern throughout the tropical Pacific Ocean ecosystem, which oscillates every 3 to 7 years [9]. These events lead to significant differences in the average temperature of the oceans, winds, surface pressure, and precipitation in parts of the Tropical Pacific Ocean [9].

Brazil has an energy matrix with a renewable-thermal configuration but essentially depends on large hydropower plants, which can be an issue in times of severe drought. For instance, Brazil had some severe droughts in the Amazon region in the years of 2005 [10], 2010 [11], and 2016 [12]. The same drought conditions were experienced in the Northeastern region in 2005, 2007, 2010, 2012, and 2016 [12,13]. Once the drought impacts are well-known, the current growth of non-hydropower plants in the country will be justified.

El Niño is associated with above average rainfall in Central Chile during winter and late spring. The La Niña is related to below average rainfall in the same period and region. El Niño is dry and La Niña is wet in Southern-Central Chile during the summer [14]. El Niño and La Niña intensities are based on the Oceanic Niño Index values [15,16].

South America is a drought hot spot in some future weather projections because of its potential to drastically react to excessive warming and drying [13,17], and El Niño events are important predictors for severe droughts over the Brazilian Amazon and Northeast [18,19]. The greatest analyzed drought, between 1982 and 2017, is an unprecedented dry period [12].

Significant local studies on the effects of ENSO in various parts of the globe have been important in establishing the prediction of solar energy [20–22]. Da Silva provides an overview study of the decrease of solar radiation for four climatic zones of northeastern Brazil, which can be attributed to the global dimming effect influenced by ENSO [23]. The variability of the solar irradiation in the Atacama Desert (northern Chile with a GHI of 3300 kWh/m^2 on latitude tilt surfaces [24]) is influenced by ENSO. These phenomena will result in years with significantly different solar irradiation than the TMY [25]. The solar radiation time series have characteristics associated with natural climatic phenomena, revealing that a reduction in solar radiation can be considered an indirect indicator of an ENSO period [26].

This brings out the following question: does ENSO uniformly impact the solar radiation in South America? The aim of this paper is to establish time series behavior changes between ENSO and the solar radiation resource spatially. These relationships may be used to guide solar radiation estimates for new solar energy plants. Therefore, the scope of this work is limited to the evaluation of the solar radiation variable. The main contributions of this paper are the discovery of a spatial pattern for the dynamic behavior of solar radiation in northeastern Brazil and the presence of extreme changes in solar radiation time series behavior in some cities due to ENSO.

2. Materials and Methods

2.1. Dataset Acquisition

All measurements represent the accumulated solar radiation per 3 h (MJ/m^2) and were provided by the Brazilian Center for Weather Forecasting and Climate Studies (CPTEC) of the National Institute for Space Research (INPE-CPTEC, http://sinda.crn.inpe.br/PCD/SITE/novo/site/index.php) and the National Agro-climatic Network (INIA Agrometeorologia, https://agrometeorologia.cl). These data were automated collected from weather stations that are widely distributed in several regions of Brazil, within the solar belt, and Chile. The chosen region has a huge potential for solar power generation. Datasets from thirty-one cities that reached a maximum threshold of 10% of lost data inside these regions were evaluated (Figure 2 and Table 1). The lost data were removed from the city datasets. An example of these raw data with blanks can be seen in Figure 3, which represents the collected data from Piatã during the El Niño, between 2015 and 2016.

This threshold was defined based on the result behavior, which presents crossovers from uncorrelated signals in a short range to correlated signals in a long range. According to [27], the global scaling exponent of positively correlated signals ($1.5 \geq \alpha > 0.5$) remains unaffected, even for a data loss of up to 90%, and shows no observable changes in the local scaling for up to 65% of the data loss. However, removing a small segment of the data strongly affects anti-correlated signals, leading to a crossover from an anti-correlated regime at a small scale to an uncorrelated regime at a large scale [28].

These data were collected within three different periods of time, each one corresponding to a full year (2920 points maximum per year, disregarding lost data) as follows. The selected period coincides with a very strong occurrence of El Niño and a strong occurrence of La Niña [9]:

- La Niña—from 1 June 2010, to 1 June 2011;
- Neutral—from 1 June 2013, to 1 June 2014;
- El Niño—from 1 June 2015, to 1 June 2016;

Table 1. Cities of the weather stations where the analyzed data were collected. Tagged cities from 1 to 25 are inside Brazil, and those from 26 to 31 are inside Chile.

Tag	State or Region	City
1	Ceará	Canindé
2	Ceará	Quixeramobim
3	Paraíba	Capim
4	Bahia	São Desidério
5	Bahia	Irecê
6	Bahia	Piatã
7	Minas Gerais	Montes Claros
8	Minas Gerais	Santa Vitória
9	Minas Gerais	Santa Fé
10	Minas Gerais	Belo Horizonte
11	Mato Grosso do Sul	Campo Grande
12	Mato Grosso do Sul	Corumbá
13	Mato Grosso do Sul	Coxim
14	Mato Grosso do Sul	Jardim
15	Pernambuco	Arcoverde
16	Pernambuco	Belém do São Francisco
17	Pernambuco	Petrolina
18	Pernambuco	São José do Egito
19	Maranhão	Açailândia
20	Maranhão	Coroatá
21	Maranhão	Riachão
22	Maranhão	Santa Inês
23	Maranhão	Urbano Santos
24	Tocantins	Chapada da Natividade
25	Goiás	Anápolis
26	Arica and Parinacota	Lluta Bajo, Arica
27	Maule	Botalcura, Pencahue
28	O'Higgins	El Tambo
29	Coquimbo	Las Rojas, La Serena
30	Maule	Los Despachos, Cauquenes
31	Bío Bío	Coronel de Maule

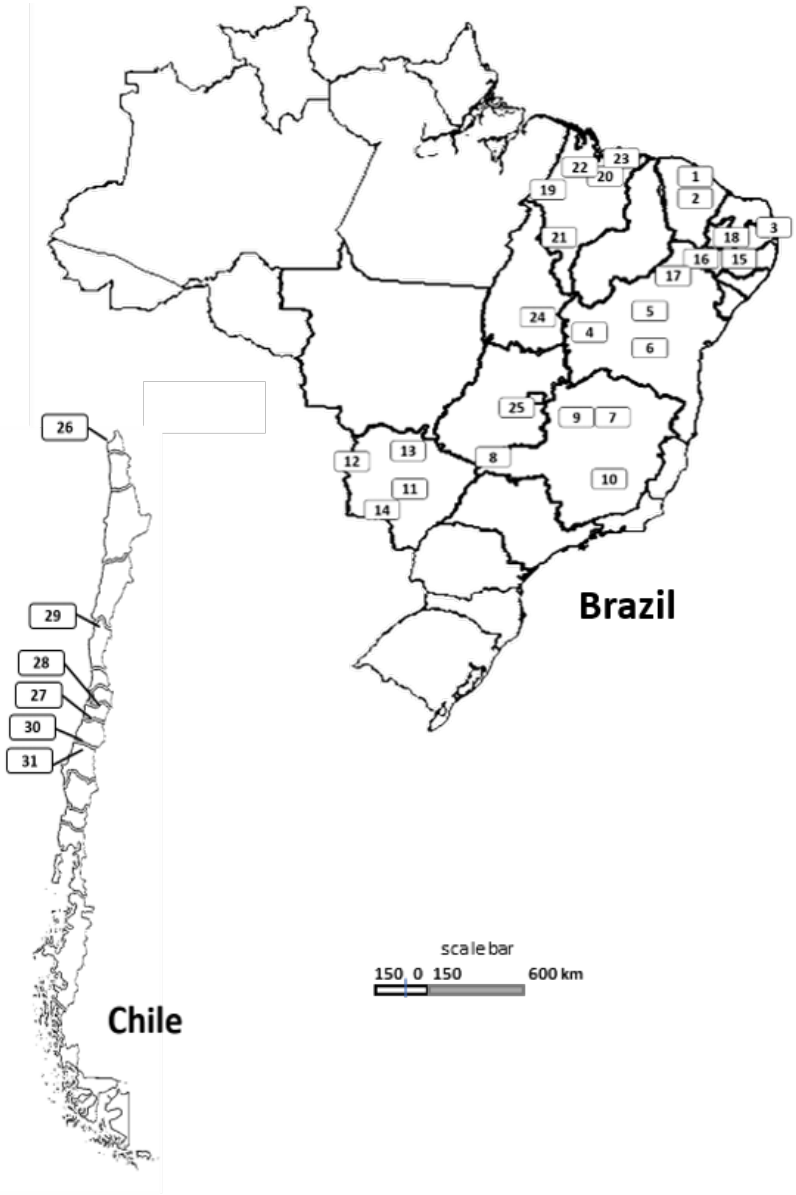

Figure 2. The accumulated solar radiation was collected from thirty-one cities in Brazil and Chile within the high potential region for solar energy production.

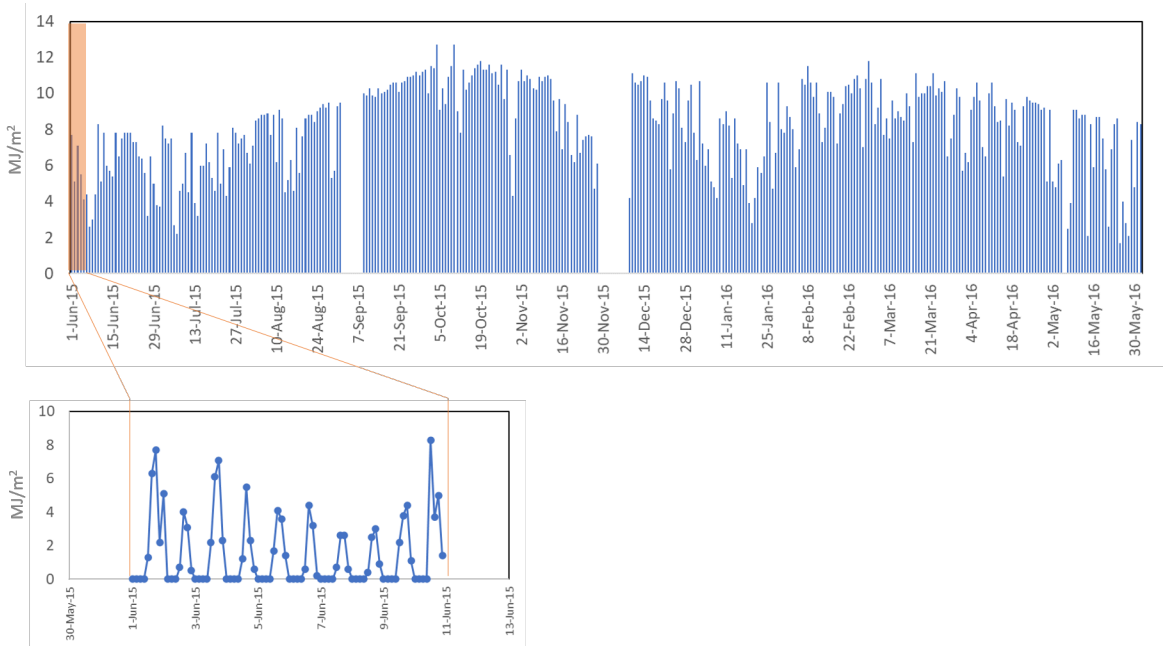

Figure 3. Raw time series of accumulated solar radiation per 3 h in Piatã, Bahia, during the El Niño period. The blanks in the chart are the lost data from weather stations.

2.2. Self-Affinity Analysis Method

Detrended Fluctuation Analysis (DFA) [29] was proposed to analyze long-range power-law correlations in nonstationary systems and extended to higher order polynomials in [30]. It has been widely applied in non-stationary time series, including the following: cloud structures evaluation [31], astrophysical systems [32], weather analyses [33–40], and solar radiation [41,42].

First order DFA (DFA1) is calculated according to the following steps. The original time series s_i is the accumulated solar radiation (MJ/m^2) per 3 h, with $i = 1, ..., N$, and N is the total number of measurements registered. The time series s_i is integrated, where $\langle s \rangle$ is the average value of s_i.

$$y(k) = \sum_{i=1}^{k} [s_i - \langle s \rangle]. \quad (1)$$

The integrated signal $y(k)$ is divided into non-overlapping boxes of equal length n; $y(k)$ is fitted using a polynomial function, which represents the trend in this box. $y(k)$ is then detrended by subtracting the local trend $y_n(k)$ within each box (k) of length n. For a given size box, the root-mean-square fluctuation, $F(n)$, is calculated as

$$F(n) = \sqrt{\frac{1}{N} \sum_{k=1}^{N} [y(k) - y_n(k)]^2}. \quad (2)$$

Equation (2) is repeated for a wide range of scales to estimate the relationship between $F(n)$ and the box size. The scaling exponent α is characterized by power law $F(n) \sim n^{\alpha}$, indicating a self-affinity parameter expressing the long-range power-law correlation properties.

Furthermore, the scaling exponent α is used to assess the long-range correlation influences on the future behavior. The α exponent is classified according to the following rules, as previously applied by [43–45]:

- anti-persistent signal ($0 < \alpha < 0.5$);
- white noise with no memory ($\alpha = 0.5$);

- persistent signal ($0.5 < \alpha < 1$);
- noise type $1/f$ ($\alpha = 1$);
- sub-diffusive process ($1 < \alpha$);
- brown noise ($\alpha = 1.5$).

A positive correlation, in time series, means that an increasing trend in the past may be followed by an increasing trend in the future. It has a persistent signal. A negative correlation means that an increasing trend in the past may be followed by a decreasing trend in the future. This signal is called anti-persistent [46].

The normal diffusion mean squared displacement of diffusing particles has a linear time dependence, one characteristic of Brownian motion and a result of the central limit theorem [47], where all steps in the diffusion process have an equal length and travel time. However, many dynamic systems mean that squared displacement presents a non-linear growth over time. A long step, called super diffusion, may be very fast, and a short step, known as sub-diffusion, may be very slow [48]. This anomalous diffusion, described by a power law, has a non-linear relation to time [49].

3. Results and Discussion

The results of the self-affinity evaluation indicated, through the correlation exponent α, the presence of crossover.

Crossover is a change point in a scaling law, where one scaling exponent applies for small scale parameters and another scaling exponent applies for large scale parameters [43,50]. The crossover points were accurately determined by the derivative of the F(n) curve for each analyzed city. The first crossover point for all curves is on $n = 9$. The second crossover point found for all curves is on $n = 80$ (10 days). Thus, based on the first derivative of the F(n) curve, the initial and final scales to fit the F(n) curve were defined, within each scale range, as follows:

- Table A1 = $n \leq 9$ ($\leq$ 27 h);
- Table A2 = $9 < n \leq 80$ ($\leq$ 10 days);
- Table A3 = $n > 80$ ($>$ 10 days).

The presence of crossovers has been found in other studies using DFA. Two different scale exponents were found in the wind speed in the Abrolhos region, Brazil. There was a sub-diffusive process in small time scales, and the process was persistent in long time scales. This is important because wind energy is directly related to solar radiation, once winds are generated by the non-uniform heating of the planet's surface [51]. The scaling exponent α for sunspots presented crossover behavior in the logÃ¢-log plot of f(t) versus time (t) [52]. The Atlantic and Pacific sea surface temperature fluctuations, for the period of 1856 to 2001, presented two pronounced scaling regimes. In the short-time regime that roughly ends at 10 months, the α of the northern Atlantic ($\approx$1.4) differs from that of the other oceans ($\approx$1.2). This behavior is distinct from the temperature fluctuations on land, where α is close to 0.65, typically above 10 days [53].

We ran hypothesis tests to assess and validate whether these data could be described as power laws. The greatest found Prob > F was $1.05623 \cdot 10^{-6}$ for the Neutral period of Petrolina, and every Pearson coefficient was greater than 0.9, thus corroborating the calculated DFA coefficients.

Firstly, α was calculated for a short range, representing a box of twenty-seven hours (Table A1 in Appendix A). For both Brazil and Chile, the coefficient was persistent in any period (ENSO or neutral), except for Capim (0.49 ± 0.01) in the neutral year and Jardim (0.49 ± 0.01) in the La Niña year, both anti-persistent but very close to the persistent interval. We recall that a linear trend was removed ($y_n(k)$) to calculate the α.

The second period was related to the DFA coefficient of solar radiation between twenty-seven hours and ten days (Table A2). Chilean evaluated cities always presented an anti-persistent coefficient. In Brazil, the α for each city was essentially anti-persistent, except for Capim (0.57 ± 0.02) and Coxim

(0.54 ± 0.01) in the neutral seasons, Santa Vitória (0.55 ± 0.03) and Urbano Santos (0.57 ± 0.01) in El Niño periods, and Jardim for all of the studied periods.

Further, the third calculated α represents a box of more than ten days (Table A3). The neutral years were consistently persistent in Brazil, except for Campo Grande (0.47 ± 0.02). Some sub-diffusive values were found for both evaluated ENSO years in São Desidério, Santa Vitória, and Coxim. Every evaluated city in Chile had persistent or sub-diffusive behavior. The smallest value was 0.70 ± 0.04, in Lluta Bajo. El Tambo, Los Despachos, and Coronel de Maule presented sub-diffusive coefficients. Besides that, El Tambo moved from persistent in the Neutral period to sub-diffusive during ENSO (Figure 4).

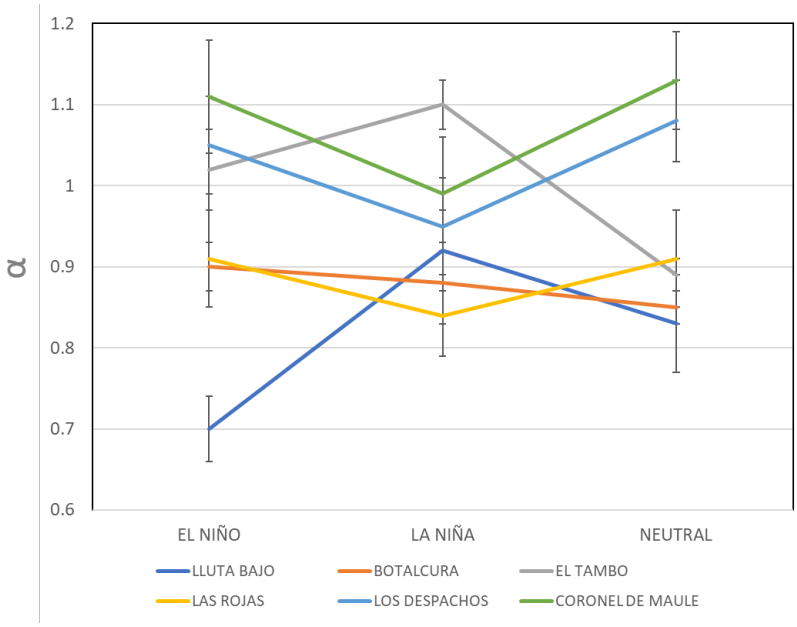

Figure 4. Chilean solar radiation range for a time scale window greater than ten days. The error bar represents one standard error of the Detrended Fluctuation Analysis (DFA) coefficient.

Moreover, some cities presented a huge range variation in the α for solar radiation (Figure 5). Coxim stands out in this evaluation, presenting the largest range in the α, changing from an anti-persistent state in El Niño periods to a sub-diffusive one during La Niña, and became persistent in the neutral year (Figure 6).

The sub-diffusive process, for a scale above 10 days, indicates dynamic behavior in the solar irradiation. This characteristic interferes with predictability in the long-term evaluation of solar radiation, and makes decisions based on those datasets. A sub-diffusive process represents a chaotic process, stated in [49,54] and proved in [55]. This factor may impact the CEPE of regions where the neutral period is persistent. Figure 7 shows the monthly accumulated solar radiation for the city of Coxim. The graph shows that an estimate of Coxim's solar radiation based on La Niña (sub-diffusive) is completely different from estimations in the Neutral period (persistent).

In contrast, in this same period, some cities presented a small range variation in α (Figure 8). Corumbá is the most stable city between the thirty-one evaluated cities. It presented the smallest range variation in the α for solar radiation during the (a) El Niño, (b) La Niña, and (c) neutral seasons, for all time scales.

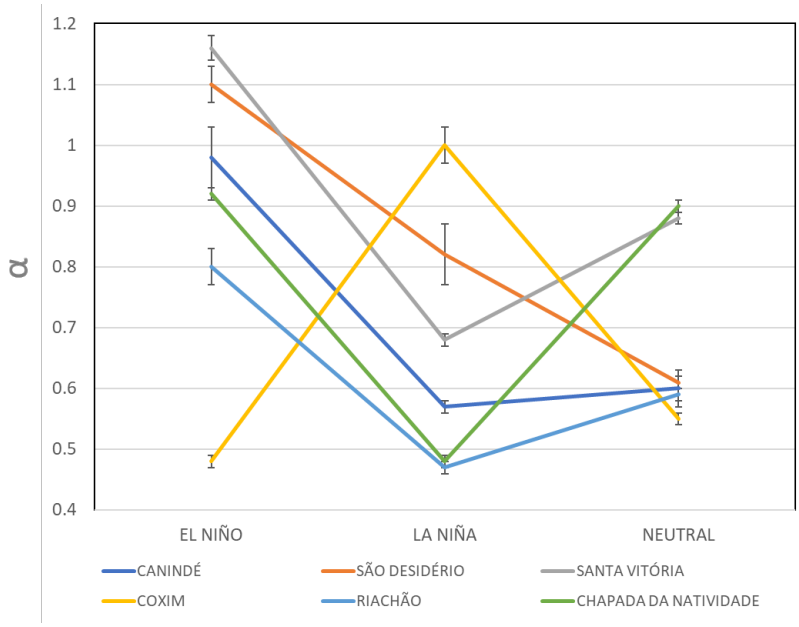

Figure 5. Cities that presented a huge range variation in the α for solar radiation for a time scale window greater than ten days. Canindé, São Desidério, and Santa Vitória were impacted by the El Niño season, moving from a persistent state to a sub-diffusive one. Coxim moved from an anti-persistent state to a sub-diffusive during the La Niña season. Chapada da Natividade were impacted by El Niña, and reached an anti-persistent α value. The error bar represents one standard error of the DFA coefficient.

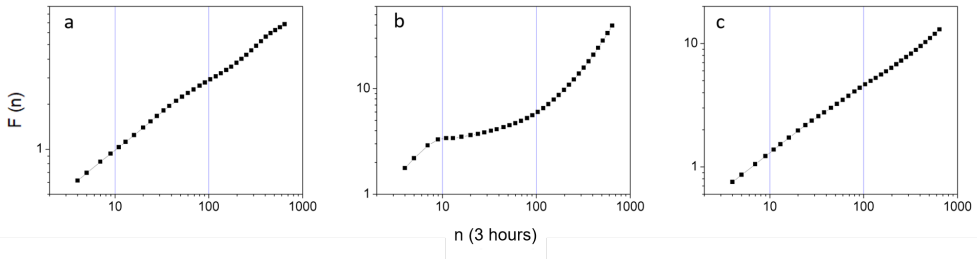

Figure 6. Coxim (MS) is the city that presented the greatest range variation in the α for solar radiation, moving from an anti-persistent state in (**a**) El Niño to a sub-diffusive one during (**b**) La Niña, and become persistent in (**c**) the neutral year, for a time scale window greater than ten days.

We used a statistical equivalence test for means with paired observations to evaluate the whole series. El Niño presented a higher mean than the Neutral and La Niña periods for a confidence level of 0.05. We cannot claim that the La Niña mean is higher than that of the Neutral periods. This reveals a statistically significant difference in El Niño DFA coefficients, systematically more persistent than the others.

In order to demonstrate the existence of spatial patterns in the alpha values, the persistence range was split in two steps (lower range of persistence = $0.50 < \alpha < 0.75$; higher range of persistence = $0.75 \leq \alpha < 1$). A Brazilian map was divided by Above the Dashed Line (ADL) and a Below the Dashed Line (BDL) regions, only for visual purposes.

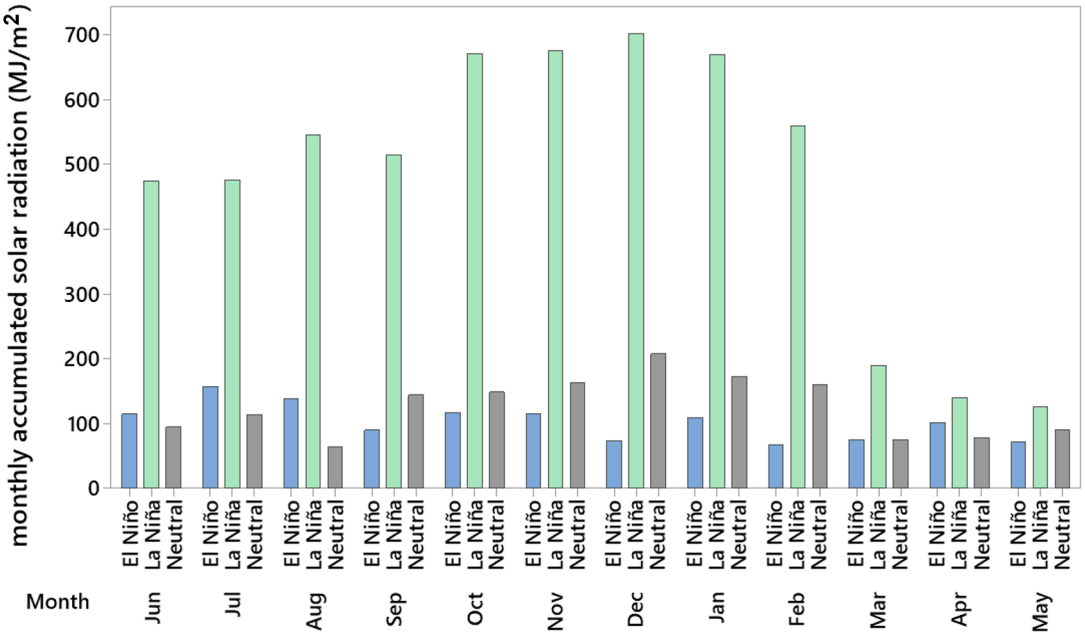

Figure 7. Monthly accumulated solar radiation for the city of Coxim. The accumulated solar radiation value is much higher in La Niña (2010–2011) than in other periods.

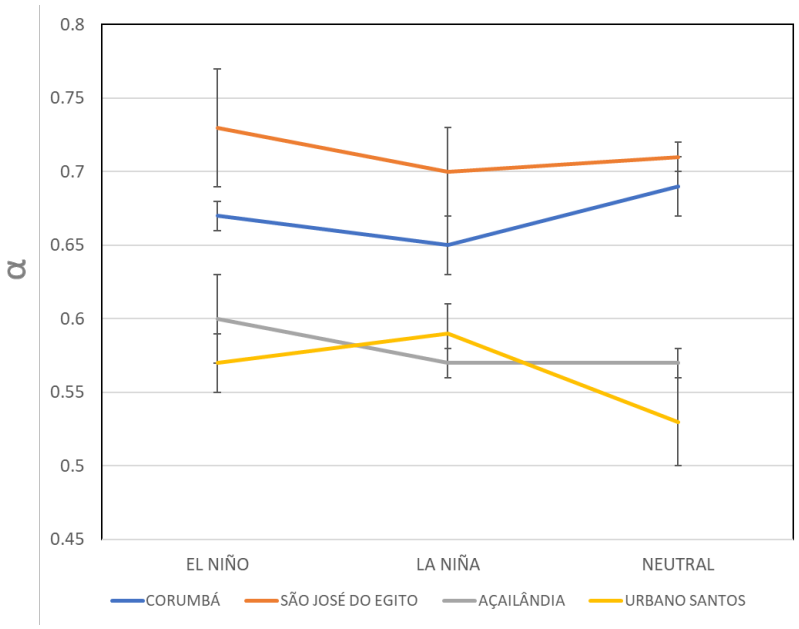

Figure 8. Cities that presented small range variations in the α for solar radiation for a time scale window greater than ten days. Corumbá, São José do Egito, Açailândia, and Urbano Santos have a persistent signal. The α, ranging through all studied seasons, never exceeded 0.05. This indicates some stability in the evaluated dataset. The error bar represents one standard error of the DFA coefficient.

Considering the Brazilian neutral period as a baseline (Figure 9c), most alpha values changed from a lower range to a higher range of persistence ADL during El Niño (Figure 9a). The La Niña period did not present the same effect ADL (Figure 9b). BDL, neither El Niño nor La Niña presented a clear pattern of changes from the baseline.

El Niño also affected the scale in the north of Chile changing the city result from a higher range on a neutral period (Figure 10c) to a lower range of persistence (Figure 10a). La Niña moved the alpha value from sub-diffusive to persistent in the cities Los Despachos and Coronel de Maule, the southernmost cities among those analyzed (Figure 10b).

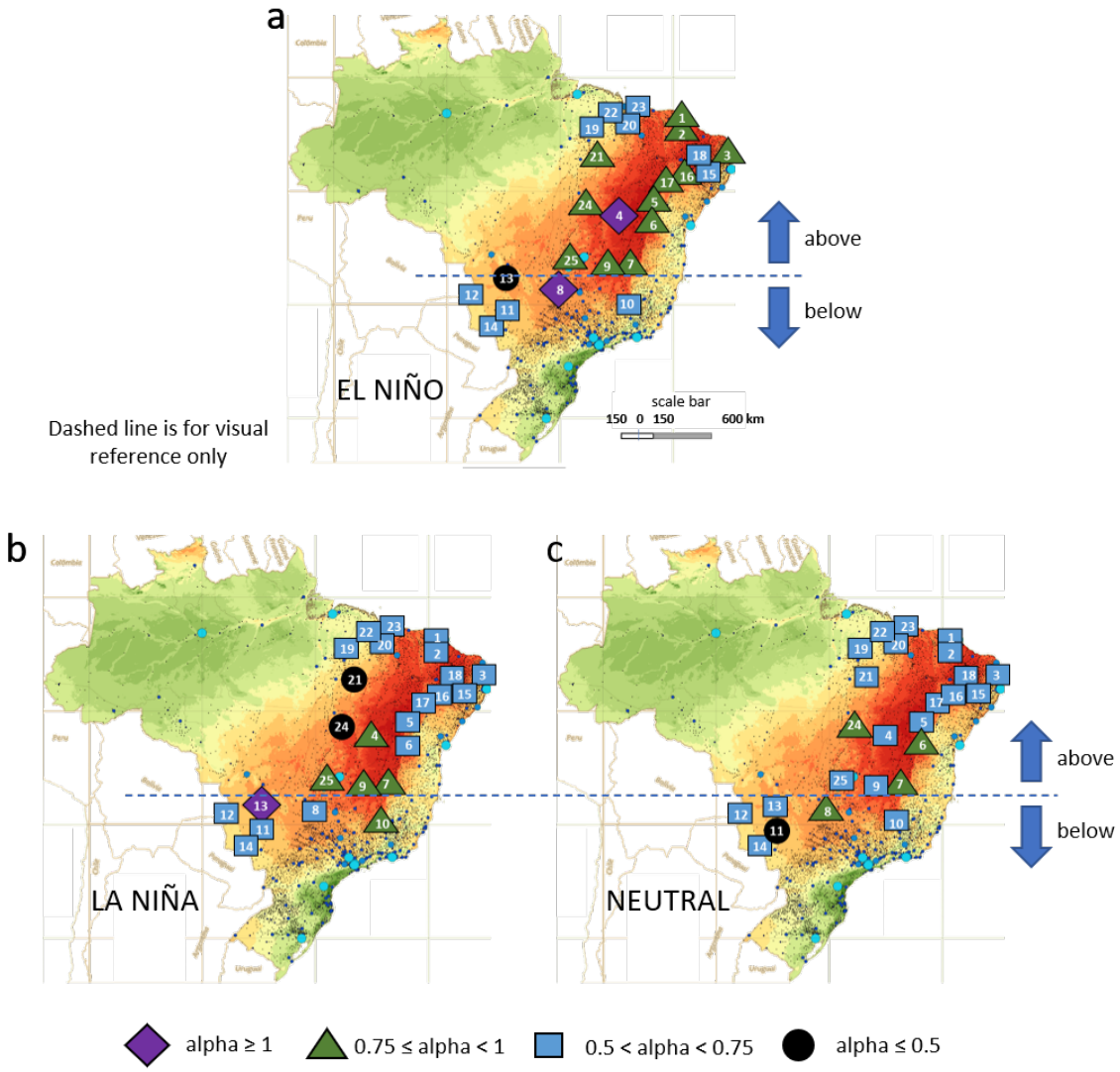

Figure 9. Spatial evaluation of α values for the El Niño (**a**), La Niña (**b**), and Neutral (**c**) periods in Brazil. The maps were divided by Above the Dashed Line (ADL) and a Below the Dashed Line (BDL) regions, only for visual purposes. Most alpha values changed from a lower range to a higher range of persistence ADL during El Niño.

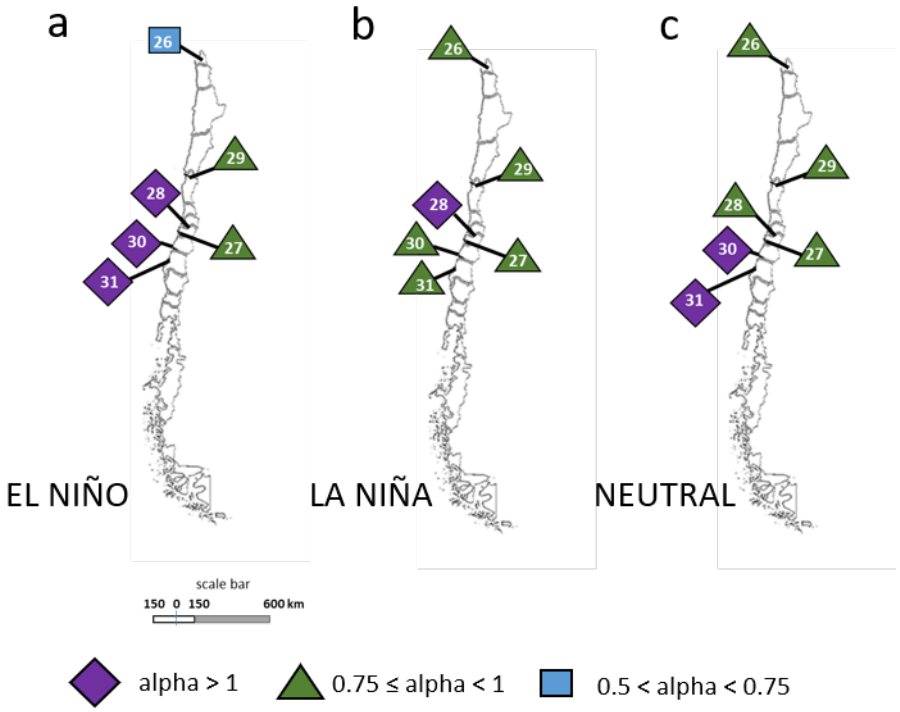

Figure 10. Spatial evaluation of α values for El Niño (**a**), La Niña (**b**), and Neutral (**c**) periods in Chile. La Niña moved the alpha value from sub-diffusive to persistent in the cities Los Despachos and Coronel de Maule, the southernmost analyzed cities.

4. Conclusions

In summary, the self-affinity of the time series for solar radiation in South America was analyzed. The neutral period was characterized mainly by the persistent behavior, determined as a desired state. However, El Niño and La Niña showed some variation in the DFA coefficient, α, sometimes moving from persistent to anti-persistent or sub-diffusive in the same city. This means that ENSO impacts the behavior of time series of solar radiation in South America.

We found that El Niño was systematically more persistent than the other periods. The impact was visually homogeneous ADL in Figure 9. This spatial pattern may be compared to rainfall in Brazil, where the North–Northeast of Brazil experiences an increase in precipitation and the South becomes dry during La Niña, while the opposite occurs in El Niño. Moreover, the results show the presence of crossover, a similar behavior found in other atmospheric variables in the region. La Niña impacted the Chilean cities of Los Despachos and Coronel de Maule, changing the α from sub-diffusive to persistent.

The sub-diffusive process indicates a dynamic series, like a transition state or transient condition. This condition may affect the evaluation of the solar plant efficiency estimate if the measurements for CEPE were collected during ENSO (i.e., Figure 7). The different behaviors found, for the same location, can lead to an assessment that does not represent the long-term solar energy potential generation, estimated for a period of ten years. This is a new implication for the prediction of large-scale generation of solar energy. This evaluation using DFA may be complementary to the other methods already in use, in order to validate the collected data.

Initially, it may be suggested that ENSO periods be avoided when collecting local data for CEPE. On the other hand, future studies should focus on the use of complex methods and the development of computational models to improve CEPE, trying to correlate neutral periods with ENSO-modified behavior. Governments may update their energy policies for solar plant projects based on this climatic behavior. Chile, for example, require new solar plant projects to be competitive in a free market [56], but a forecast based on a sub-diffusive behavior may lead to a wrong decision.

To the best of our knowledge, this is the first time that the self-affinity of solar radiation has been evaluated in a large area of South America, revealing changes in the time series fluctuation affecting the climatic behavior of the region due to ENSO. This evaluation is a starting point to understanding the ENSO effects on solar plant projects, where time series in the same location are compared. Future studies may evaluate the cross-correlation between solar radiation, temperature, humidity, and wind time series, during ENSO and neutral periods, for each weather station.

Author Contributions: T.B.M.: conceptualization, methodology, software, validation, formal analysis, investigation, data curation, writing—original draft, writing—review and editing, and supervision. A.S.N.F.: conceptualization, methodology, software, validation, formal analysis, investigation, data curation, writing—original draft, and writing—review and editing. M.A.M.: conceptualization, resources, project administration, visualization, investigation, writing—review and editing, supervision, and funding acquisition. S.P.: Methodology, Software, Validation, Formal analysis, and writing—review and editing. A.A.B.S.: conceptualization, resources, project administration, writing—review and editing, and funding acquisition. All authors have read and agreed to the published version of the manuscript.

Funding: This work received financial support from the National Counsel of Technological and Scientific Development, CNPq (grant number 305291/2018-1 and 431651/2018-3).

Conflicts of Interest: The authors declare that there is no conflict of interest.

Appendix A. Output Data

Table A1. The DFA coefficient (α) of solar radiation in less than twenty-seven hours.

Tag	El Niño	Error	La Niña	Error	Neutral	Error
1	0.74	0.06	0.77	0.06	0.77	0.06
2	0.79	0.07	0.78	0.06	0.71	0.06
3	0.56	0.01	0.79	0.07	0.49	0.01
4	0.80	0.07	0.79	0.07	0.79	0.07
5	0.80	0.07	0.78	0.07	0.79	0.07
6	0.80	0.07	0.78	0.07	0.77	0.07
7	0.78	0.07	0.77	0.06	0.78	0.07
8	0.62	0.04	0.78	0.07	0.70	0.05
9	0.79	0.07	0.79	0.07	0.79	0.07
10	0.79	0.07	0.79	0.07	0.78	0.07
11	0.79	0.06	0.79	0.07	0.80	0.07
12	0.79	0.07	0.79	0.07	0.79	0.07
13	0.51	0.01	0.78	0.06	0.59	0.00
14	0.62	0.00	0.49	0.01	0.61	0.00
15	0.74	0.05	0.75	0.06	0.76	0.06
16	0.77	0.06	0.80	0.07	0.79	0.07
17	0.81	0.07	0.80	0.07	0.80	0.07
18	0.80	0.07	0.77	0.07	0.77	0.07
19	0.77	0.06	0.76	0.06	0.76	0.06
20	0.80	0.07	0.79	0.07	0.77	0.07
21	0.79	0.07	0.50	0.00	0.78	0.07
22	0.78	0.07	0.77	0.06	0.79	0.07
23	0.66	0.00	0.78	0.07	0.78	0.07
24	0.72	0.01	0.85	0.08	0.80	0.07
25	0.78	0.06	0.77	0.06	0.77	0.06
26	0.78	0.07	0.79	0.07	0.79	0.07
27	0.84	0.08	0.83	0.07	0.81	0.07
28	0.83	0.08	0.57	0.06	0.78	0.07
29	0.81	0.07	0.80	0.07	0.81	0.07
30	0.84	0.08	0.84	0.08	0.84	0.08
31	0.84	0.08	0.84	0.08	0.85	0.08

Table A2. The DFA coefficient (α) of solar radiation between twenty seven hours and ten days.

Tag	El Niño	Error	La Niña	Error	Neutral	Error
1	NA	0.01	0.19	0.01	0.23	0.01
2	NA	0.01	0.21	0.01	NA	0.02
3	0.46	0.01	0.21	0.02	0.57	0.02
4	0.23	0.02	0.14	0.01	0.24	0.03
5	NA	0.01	0.22	0.02	0.21	0.01
6	0.20	0.02	0.22	0.02	0.22	0.02
7	0.18	0.02	0.20	0.02	0.24	0.02
8	0.55	0.03	0.22	0.02	0.35	0.03
9	0.16	0.02	0.19	0.02	0.23	0.02
10	0.25	0.02	0.24	0.02	0.31	0.02
11	0.30	0.02	0.26	0.02	NA	0.02
12	0.24	0.02	0.27	0.02	0.27	0.02
13	0.48	0.01	0.22	0.01	0.54	0.00
14	0.55	0.01	0.57	0.00	0.50	0.01
15	0.23	0.01	0.22	0.01	0.20	0.01
16	NA	0.01	0.15	0.02	0.15	0.01
17	0.10	0.01	0.22	0.01	0.16	0.02
18	0.14	0.01	0.21	0.01	0.20	0.02
19	0.21	0.01	0.27	0.01	0.23	0.01
20	NA	0.01	0.17	0.01	0.23	0.02
21	0.19	0.02	0.49	0.00	0.23	0.02
22	0.16	0.01	0.18	0.01	0.18	0.01
23	0.57	0.01	0.19	0.01	0.20	0.01
24	NA	0.00	0.28	0.02	NA	0.03
25	0.19	0.02	0.20	0.02	0.23	0.02
26	0.11	0.01	0.08	0.01	0.07	0.01
27	0.33	0.02	0.39	0.02	0.34	0.02
28	0.25	0.02	NA	0.02	0.22	0.02
29	0.17	0.01	0.17	0.01	0.16	0.01
30	0.21	0.02	0.22	0.02	0.17	0.02
31	0.18	0.02	0.21	0.02	0.14	0.02

Table A3. The DFA coefficient (α) of solar radiation for more than ten days.

Tag	El Niño	Error	La Niña	Error	Neutral	Error
1	0.98	0.05	0.57	0.01	0.60	0.03
2	0.77	0.03	0.63	0.01	0.61	0.01
3	0.85	0.03	0.61	0.02	0.67	0.01
4	1.10	0.03	0.82	0.05	0.61	0.01
5	0.77	0.04	0.64	0.01	0.72	0.02
6	0.84	0.04	0.66	0.01	0.79	0.01
7	0.81	0.02	0.88	0.03	0.78	0.02
8	1.16	0.02	0.68	0.01	0.88	0.01
9	0.77	0.01	0.81	0.00	0.68	0.01
10	0.70	0.01	0.84	0.02	0.75	0.02
11	0.62	0.00	0.73	0.01	0.47	0.02
12	0.67	0.00	0.65	0.02	0.69	0.02
13	0.48	0.01	1.00	0.03	0.55	0.01
14	0.74	0.03	0.55	0.00	0.52	0.02
15	0.59	0.03	0.52	0.02	0.54	0.01
16	0.76	0.04	0.62	0.02	0.61	0.01
17	0.91	0.04	0.65	0.01	0.69	0.01
18	0.73	0.04	0.70	0.03	0.71	0.01
19	0.60	0.03	0.57	0.01	0.57	0.01
20	0.70	0.03	0.61	0.04	0.70	0.02

Table A3. *Cont.*

Tag	El Niño	Error	La Niña	Error	Neutral	Error
21	0.80	0.03	0.47	0.01	0.59	0.01
22	0.63	0.02	0.52	0.02	0.63	0.03
23	0.57	0.02	0.59	0.02	0.53	0.03
24	0.92	0.01	0.48	0.01	0.90	0.00
25	0.76	0.00	0.81	0.02	0.65	0.01
26	0.70	0.04	0.92	0.05	0.83	0.06
27	0.90	0.03	0.88	0.05	0.85	0.02
28	1.02	0.05	1.10	0.03	0.89	0.02
29	0.91	0.06	0.84	0.05	0.91	0.06
30	1.05	0.06	0.95	0.06	1.08	0.05
31	1.11	0.07	0.99	0.07	1.13	0.06

References

1. Millais, C. *Relatório Wind Force 12: Segurança Global a Partir do Vento*; n. 104; Revista ECO: Rio de Janeiro, Brazil, 2005.
2. Ezzati, M.; Bailis, R.; Kammen, D.M.; Holloway, T.; Price, L.; Cifuentes, L.A.; Barnes, B.; Chaurey, A.; Dhanapala, K.N. Energy management and global health. *Annu. Rev. Environ. Resour.* **2004**, *29*, 383–419. [CrossRef]
3. Libra, M.; Daneček, M.; Lešetickỳ, J.; Poulek, V.; Sedláček, J.; Beránek, V. Monitoring of Defects of a Photovoltaic Power Plant Using a Drone. *Energies* **2019**, *12*, 795. [CrossRef]
4. Beránek, V.; Olšan, T.; Libra, M.; Poulek, V.; Sedláček, J.; Dang, M.Q.; Tyukhov, I.I. New monitoring system for photovoltaic power plantsâ€™ management. *Energies* **2018**, *11*, 2495. [CrossRef]
5. Manuel Godinho Rodrigues, E.; Godina, R.; Marzband, M.; Pouresmaeil, E. Simulation and comparison of mathematical models of PV cells with growing levels of complexity. *Energies* **2018**, *11*, 2902. [CrossRef]
6. Bento, P.; Nunes, H.; Pombo, J.; Calado, M.d.R.; Mariano, S. Daily operation optimization of a hybrid energy system considering a short-term electricity price forecast scheme. *Energies* **2019**, *12*, 924. [CrossRef]
7. EPE. *2017 Statistical Yearbook of ele3ctricity: 2016 ba3seline 3year*; Technical report; EPE: Brasilia, Brazil, 2016.
8. Pereira, E.B.; Martins, F.R.; Gonçalves, A.R.; Costa, R.S.; Lima, F.J.L.d.; Ruther, R.; Abreu, S.L.d.; Tiepolo, G.M.; Pereira, S.V.; Souza, J.G.d. *Atlas Brasileiro de Energia Solar*; Instituto Nacional de Pesquisas Espaciais, INPE: Sao Jose Dos Campos, Brazil, 2017.
9. NOAA. National Oceanic and Atmospheric Administration. 2018. Available online: https://www.noaa.gov/education/resource-collections/weather-atmosphere/el-nino (accessed on 4 November 2019).
10. Phillips, O.L.; Aragão, L.E.O.C.; Lewis, S.L.; Fisher, J.B.; Lloyd, J.; López-González, G.; Malhi, Y.; Monteagudo, A.; Peacock, J.; Quesada, C.A.; et al. Drought Sensitivity of the Amazon Rainforest. *Science* **2009**, *323*, 1344–1347. [CrossRef] [PubMed]
11. Lewis, S.L.; Brando, P.M.; Phillips, O.L.; van der Heijden, G.M.F.; Nepstad, D. The 2010 Amazon Drought. *Science* **2011**, *331*, 554. [CrossRef] [PubMed]
12. Erfanian, A.; Wang, G.; Fomenko, L. Unprecedented drought over tropical South America in 2016: significantly under-predicted by tropical SST. *Sci. Rep.* **2017**, *7*, 5811. [CrossRef]
13. Marengo, J.A.; Torres, R.R.; Alves, L.M. Drought in Northeast Brazil—Past, present, and future. *Theor. Appl. Climatol.* **2017**, *129*, 1189–1200. [CrossRef]
14. Montecinos, A.; Aceituno, P. Seasonality of the ENSO-related rainfall variability in central Chile and associated circulation anomalies. *J. Clim.* **2003**, *16*, 281–296. [CrossRef]
15. Cai, W.; Wang, G.; Santoso, A.; McPhaden, M.J.; Wu, L.; Jin, F.F.; Timmermann, A.; Collins, M.; Vecchi, G.; Lengaigne, M.; et al. Increased frequency of extreme La Niña events under greenhouse warming. *Nat. Clim. Chang.* **2015**, *5*, 132. [CrossRef]
16. Wang, B.; Chan, J.C. How strong ENSO events affect tropical storm activity over the western North Pacific. *J. Clim.* **2002**, *15*, 1643–1658. [CrossRef]

17. Cox, P.M.; Harris, P.P.; Huntingford, C.; Betts, R.A.; Collins, M.; Jones, C.D.; Jupp, T.E.; Marengo, J.A.; Nobre, C.A. Increasing risk of Amazonian drought due to decreasing aerosol pollution. *Nature* **2008**, *453*, 212. [CrossRef]
18. Hastenrath, S. Predictability of north-east Brazil droughts. *Nature* **1984**, *307*, 531. [CrossRef]
19. Marengo, J.A. Interdecadal variability and trends of rainfall across the Amazon basin. *Theor. Appl. Climatol.* **2004**, *78*, 79–96. [CrossRef]
20. Davy, R.; Troccoli, A. Interannual variability of solar energy generation in Australia. *Sol. Energy* **2012**, *86*, 3554–3560. [CrossRef]
21. Mohammadi, K.; Goudarzi, N. Association of direct normal irradiance with El Niño Southern Oscillation and its consequence on concentrated solar power production in the US Southwest. *Appl. Energy* **2018**, *212*, 1126–1137. [CrossRef]
22. Chang, T.P.; Liu, F.J.; Ko, H.H.; Huang, M.C. Oscillation characteristic study of wind speed, global solar radiation and air temperature using wavelet analysis. *Appl. Energy* **2017**, *190*, 650–657. [CrossRef]
23. da Silva, V.d.P.; e Silva, R.A.; Cavalcanti, E.P.; Braga, C.C.; de Azevedo, P.V.; Singh, V.P.; Pereira, E.R.R. Trends in solar radiation in NCEP/NCAR database and measurements in northeastern Brazil. *Sol. Energy* **2010**, *84*, 1852–1862. [CrossRef]
24. Fthenakis, V.; Atia, A.A.; Perez, M.; Florenzano, A.; Grageda, M.; Lofat, M.; Ushak, S.; Palma, R. Prospects for photovoltaics in sunny and arid regions: A solar grand plan for chile-part i-investigation of pv and wind penetration. In Proceedings of the 2014 IEEE 40th Photovoltaic Specialist Conference (PVSC), Denver, CO, USA, 8–13 June 2014; pp. 1424–1429.
25. Bravo1, R.; Friedrich, D. Two-stage optimisation of hybrid solar power plants. *Sol. Energy* **2018**, *164*, 187–199. [CrossRef]
26. Papadimas, C.D.; Fotiadi, A.K.; Hatzianastassiou, N.; Vardavas, I.; Bartzokas, A. Regional coâ€variability and teleconnection patterns in surface solar radiation on a planetary scale. *Int. J. Climatol.* **2010**, *30*, 2314–2329. [CrossRef]
27. Ma, Q.D.; Bartsch, R.P.; Bernaola-Galván, P.; Yoneyama, M.; Ivanov, P.C. Effect of extreme data loss on long-range correlated and anticorrelated signals quantified by detrended fluctuation analysis. *Phys. Rev. E* **2010**, *81*, 031101. [CrossRef] [PubMed]
28. Chen, Z.; Ivanov, P.C.; Hu, K.; Stanley, H.E. Effect of nonstationarities on detrended fluctuation analysis. *Phys. Rev. E* **2002**, *65*, 041107. [CrossRef]
29. Peng, C.K.; Buldyrev, S.V.; Havlin, S.; Simons, M.; Stanley, H.E.; Goldberger, A.L. Mosaic organization of DNA nucleotides. *Phys. Rev. E* **1994**, *49*, 1685. [CrossRef]
30. Hu, K.; Ivanov, P.C.; Chen, Z.; Carpena, P.; Stanley, H.E. Effect of trends on detrended fluctuation analysis. *Phys. Rev. E* **2001**, *64*, 011114. [CrossRef] [PubMed]
31. Ivanova, K.; Ausloos, M.; Clothiaux, E.; Ackerman, T. Break-up of stratus cloud structure predicted from non-Brownian motion liquid water and brightness temperature fluctuations. *EPL (Europhys. Lett.)* **2000**, *52*, 40. [CrossRef]
32. Moret, M.A.; Zebende, G.; Nogueira Jr, E.; Pereira, M. Fluctuation analysis of stellar X-ray binary systems. *Phys. Rev. E* **2003**, *68*, 041104. [CrossRef]
33. de Oliveira Santos, M.; Stosic, T.; Stosic, B.D. Long-term correlations in hourly wind speed records in Pernambuco, Brazil. *Phys. A Stat. Mech. Appl.* **2012**, *391*, 1546–1552. [CrossRef]
34. Govindan, R.; Kantz, H. Long-term correlations and multifractality in surface wind speed. *EPL (Europhys. Lett.)* **2004**, *68*, 184. [CrossRef]
35. Kavasseri, R.G.; Nagarajan, R. A multifractal description of wind speed records. *Chaos Solitons Fractals* **2005**, *24*, 165–173. [CrossRef]
36. Koçak, K. Examination of persistence properties of wind speed records using detrended fluctuation analysis. *Energy* **2009**, *34*, 1980–1985. [CrossRef]
37. Kurnaz, M. Application of detrended fluctuation analysis to monthly average of the maximum daily temperatures to resolve different climates. *Fractals* **2004**, *12*, 365–373. [CrossRef]
38. Chen, X.; Lin, G.; Fu, Z. Long-range correlations in daily relative humidity fluctuations: A new index to characterize the climate regions over China. *Geophys. Res. Lett.* **2007**, *34*. [CrossRef]
39. Matsoukas, C.; Islam, S.; Rodriguez-Iturbe, I. Detrended fluctuation analysis of rainfall and streamflow time series. *J. Geophys. Res. Atmos.* **2000**, *105*, 29165–29172. [CrossRef]

40. Talkner, P.; Weber, R.O. Power spectrum and detrended fluctuation analysis: Application to daily temperatures. *Phys. Rev. E* **2000**, *62*, 150. [CrossRef] [PubMed]
41. Zeng, Z.; Yang, H.; Zhao, R.; Meng, J. Nonlinear characteristics of observed solar radiation data. *Sol. Energy* **2013**, *87*, 204–218. [CrossRef]
42. Madanchi, A.; Absalan, M.; Lohmann, G.; Anvari, M.; Tabar, M.R.R. Strong short-term non-linearity of solar irradiance fluctuations. *Sol. Energy* **2017**, *144*, 1–9. [CrossRef]
43. Peng, C.K.; Havlin, S.; Stanley, H.E.; Goldberger, A.L. Quantification of scaling exponents and crossover phenomena in nonstationary heartbeat time series. *Chaos Interdiscip. J. Nonlinear Sci.* **1995**, *5*, 82–87. [CrossRef]
44. Malamud, B.D.; Turcotte, D.L. Self-affine time series: Measures of weak and strong persistence. *J. Stat. Plan. Inference* **1999**, *80*, 173–196. [CrossRef]
45. Galhardo, C.; Penna, T.; de Menezes, M.A.; Soares, P. Detrended fluctuation analysis of a systolic blood pressure control loop. *New J. Phys.* **2009**, *11*, 103005. [CrossRef]
46. Delignières, D.; Torre, K.; Bernard, P.L. Transition from persistent to anti-persistent correlations in postural sway indicates velocity-based control. *PLoS Comput. Biol.* **2011**, *7*, e1001089. [CrossRef]
47. Réveillac, A. Estimation of quadratic variation for two-parameter diffusions. *Stoch. Process. Their Appl.* **2009**, *119*, 1652–1672. [CrossRef]
48. Sharifi-Viand, A.; Mahjani, M.; Jafarian, M. Investigation of anomalous diffusion and multifractal dimensions in polypyrrole film. *J. Electroanal. Chem.* **2012**, *671*, 51–57. [CrossRef]
49. Havlin, S.; Ben-Avraham, D. Diffusion in disordered media. *Adv. Phys.* **2002**, *51*, 187–292. [CrossRef]
50. Kantelhardt, J.W. Fractal and multifractal time series. In *Encyclopedia of Complexity and Systems Science*; Springer: New York, NY, USA, 2009; pp. 3754–3779.
51. Santos, J.; Moreira, D.; Moret, M.; Nascimento, E. Analysis of long-range correlations of wind speed in different regions of Bahia and the Abrolhos Archipelago, Brazil. *Energy* **2019**, *167*, 680–687. [CrossRef]
52. Moret, M. Self-affinity and nonextensivity of sunspots. *Phys. Lett. A* **2014**, *378*, 494–496. [CrossRef]
53. Monetti, R.A.; Havlin, S.; Bunde, A. Long-term persistence in the sea surface temperature fluctuations. *Phys. A Stat. Mech. Appl.* **2003**, *320*, 581–589. [CrossRef]
54. Viswanathan, G.M.; Da Luz, M.G.; Raposo, E.P.; Stanley, H.E. *The Physics of Foraging: An Introduction to Random Searches and Biological Encounters*; Cambridge University Press: New York, NY, USA, 2011.
55. Nascimento Filho, A.; de Souza, J.; Pereira, A.; Santos, A.; da Cunha Lima, I.; da Cunha Lima, A.; Moret, M. Comparative analysis on turbulent regime: A self-affinity study in fluid flow by using OpenFoam CFD. *Phys. A Stat. Mech. Appl.* **2017**, *474*, 260–266. [CrossRef]
56. Grágeda, M.; Escudero, M.; Alavia, W.; Ushak, S.; Fthenakis, V. Review and multi-criteria assessment of solar energy projects in Chile. *Renew. Sustain. Energy Rev.* **2016**, *59*, 583–596. [CrossRef]